Article

Design and Testing of Vehicle-Mounted Crop Growth Monitoring System

Shanshan Yu [1,2,3,4,5,6], Qiang Cao [1,3,4,5,6], Yongchao Tian [1,3,4,5,6], Yan Zhu [1,3,4,5,6], Xiaojun Liu [1,3,4,5,6], Jun Ni [1,3,4,5,6], Wenyi Zhang [2] and Weixing Cao [1,3,4,5,6,*]

1   National Engineering and Technology Center for Information Agriculture, Nanjing Agricultural University, Nanjing 210095, China; yushanshan@caas.cn (S.Y.); qiangcao@njau.edu.cn (Q.C.); yctian@njau.edu.cn (Y.T.); yanzhu@njau.edu.cn (Y.Z.); liuxj@njau.edu.cn (X.L.); nijun@njau.edu.cn (J.N.)
2   Nanjing Institute of Agricultural Mechanization, Ministry of Agriculture and Rural Affairs, Nanjing 210014, China; zwy-yxkj@163.com
3   MOE Engineering Research Center of Smart Agricultural, Nanjing Agricultural University, Nanjing 210095, China
4   MARA Key Laboratory for Crop System Analysis and Decision Making, Nanjing Agricultural University, Nanjing 210095, China
5   Jiangsu Key Laboratory for Information Agriculture, Nanjing Agricultural University, Nanjing 210095, China
6   Institute of Smart Agriculture, Nanjing Agricultural University, Nanjing 210095, China
*   Correspondence: caow@njau.edu.cn; Tel.: +86-25-8439-6804; Fax: +86-25-8439-6672

Abstract: The aim of this study was to overcome the impact of vibration generated by agricultural machinery on the monitoring accuracy and performance of vehicle-mounted crop growth monitoring systems during field operation. This paper developed a vehicle-mounted crop growth monitoring system with vibration damping capability to achieve this goal. The system consists of a multispectral crop growth sensor, signal conditioning module, and truss-type sensor bracket with self-vibration damping capability. The commercial finite element analysis software ABAQUS 6.10 was used to conduct modal and dynamic simulation analyses of the sensor bracket, which indicate that the truss-type sensor bracket can damp vibrations effectively. The *p*-values (least significant differences) of crop canopy DNRE (red edge normalized difference vegetation index) under different operating speeds (1.5, 3, and 4.5 km/h) are 0.454, 0.703, 0.81, and 0.838, respectively, for four different crop growth stages. In a comparative experiment between the proposed monitoring system and two similar vehicle-mounted sensors (CropSpec and GreenSeeker RT 200) for measuring agronomic parameters at different stages of crop growth, the proposed monitoring system yielded R2 values of 0.8757, 0.7194, and 0.795, respectively, and RMSE values of 0.7157, 2.2341, and 2.0952, respectively, in the tillering stage, jointing stage, and tillering and jointing stage, outperforming the other two sensors.

Keywords: vehicle-mounted monitoring system; signal conditioning; sensor bracket; self-vibration damping; simulation analysis

1. Introduction

As a means to improve soil fertility, fertilization is an important measure to improve grain yield per unit area [1–3]. However, the excessive application of chemical fertilizer will not only reduce the utilization efficiency of fertilizer, reduce the organic matter in the soil, harden cultivated land, and acidify soil, but also aggravate non-point source pollution and increase the cost of agricultural production [4–6]. Therefore, it is desirable to apply appropriate amounts of fertilizer according to the needs at individual field locations.

Precision fertilization is to scientifically and accurately apply fertilizer according to the actual demand calculated according to multiple factors, including the fertilizer demand in each growth stage and the difference between the spatial distribution of local soil conditions and that of crop growth [7–9]. There are two fundamental approaches of

variable-rate technology (VRT): (i) map-based and (ii) sensor-based systems. In the map-based approach, fertilizer may be placed at different locations than the prescribed points on an application map due to the inaccuracy of the positioning system and/or the longer than anticipated response time of the machine actuation [10–13]. Therefore, it is more desirable to have a vehicle-mounted sensing system that is able to monitor the physical and chemical characteristics of plants and control VRT application of fertilizer according to plant needs in real time in situ [14,15].

Variable-rate fertilization systems based on vehicle-mounted sensors have stringent requirements on response time (i.e., the period from the moment of transmitting monitoring data to the moment of the actuator performing the variable-rate fertilization operation). To simplify the sensor monitoring data and reduce the data processing time, researchers have conducted extensive research on vehicle-mounted crop growth monitoring sensor systems working in crop growth's sensitive and characteristic wavelength bands. Some of the research results have been turned into commercial products. Stone et al. [16] fitted a spectral sensor to a tractor to measure the spectral reflectance of wheat at the wavelength bands of 671 nm and 780 nm, and established the plant nitrogen spectral index (PNSI) using the absolute value of the reciprocal of the normalized difference vegetation index (NDVI). The results showed that there was a good correlation between crop nitrogen content and the PNSI. This work paved the way for developing the GreenSeeker(NTech Industries Inc., Ukiah, CA, USA) NDVI active light source sensor, the fruit of joint R&D by Oklahoma State University and NTech (the product was put on the market in 2001). Link et al. [17] developed the Hydro-N vehicle-mounted passive sensor and made use of the NDVI to monitor the nitrogen content of the crop. This sensor is the predecessor of the Yara-N sensor(Yara International Inc., Oslo, Norway). Holland et al. [18] developed the Crop Circle(Holland Scientific Inc., Lincoln, NE, USA) active light source sensor, which uses the reflectance values obtained in the green band and near-infrared band to estimate the nitrogen content of the crop. The reason for the use of the reflectance in the green band instead of the red band is as follows: when the leaf area index of the crop exceeds 2.0, the GNVI is more sensitive to the changes in chlorophyll concentration and crop yield than the NDVI. Other commercialized products available in the market include the OptRx sensor developed and produced by Ag Leader Technology (Ames, IA, USA) and the CropSpec active light source sensor developed and produced by Topcon (Tokyo, Japan), reducing fertilizer consumption, increasing crop yield, and increasing farmers' incomes [19]. Meanwhile, the research also promotes the application of variable-rate fertilization systems based on vehicle-mounted sensors [20]. At present, the research on vehicle-mounted crop growth monitoring systems focuses on the empirical study of the field sensing performance of vehicle-mounted sensors and the construction of quantitative models for monitoring different agronomic parameters [21]. The vehicle-mounted sensors are usually directly fixed to the cantilever beam of agricultural machinery such as tractors, spray vehicles, etc. When the carrier agricultural machine is working in the field, the sensor bracket will experience strong vibration due to the engine vibration of the machine, the undulation of the plot, and the softness of the soil. In particular, as cantilever brackets are highly flexible, the weak vibration of agricultural machinery will lead to strong vibration and elastic deformation at the end of the cantilever bracket, which will affect the sensing performance and accuracy of the vehicle-mounted crop growth sensors installed at the end of the cantilever bracket [15]. Therefore, there is an urgent need to design sensor brackets with self-vibration damping capability.

The vibration excitation source of the sensor bracket for installing vehicle-mounted crop growth sensors is agricultural machinery, so the vibration of the sensor bracket belongs to forced vibration, and the vibration responses include stress, displacement, and acceleration response. The finite element method (FEM) is widely used to solve the vibration characteristics of mechanical structures [22–31]. The nonlinear mechanical mechanism dynamics FEM is used to solve dynamic problems of mechanical structures involving nonlinear factors such as geometry, material, or state [32]. Patrik et al. [33] used

the nonlinear FEM to analyze the vibration dynamic response of the end section of three types of booms: fixed, pendulum suspension, and trapezoidal suspension. Qiu et al. [34] and He et al. [35] carried out modal analysis and elastic deformation analysis on the spray bar of a spray vehicle using the FEM. Chen [36] simulated the dynamic characteristics of a flexible truss spray bar system using the FEM. Chen et al. [37] simulated and analyzed the dynamic characteristics of the frame of a spray bar spray vehicle based on the FEM and designed a damping system based on the analysis results. It can be seen that it is feasible to design a sensor bracket and analyze its self-vibration damping performance based on the FEM.

This study aims to simulate and analyze the vibrational characteristics of a vehicle-mounted crop growth monitoring system during field operation. Based on modal and dynamic simulation analysis, a truss-type sensor bracket with self-vibration damping capability was developed. Moreover, a module for sensor signal conditioning with amplification and noise filtering functions was developed. By integrating the advantages of the truss-type bracket and the signal conditioning module, the impact of vibration of agricultural machinery on the monitoring performance of the vehicle-mounted crop growth sensor is mitigated.

2. Materials and Methods

The proposed vehicle-mounted crop growth monitoring system consists of a vehicle-mounted crop growth sensor, sensor bracket, and sensor signal conditioning module. The vehicle-mounted crop growth monitoring system is installed on an agricultural machine through the sensor bracket. The impact of vibration of agricultural machinery on the monitoring performance of the vehicle-mounted crop growth sensor is mitigated jointly by the self-vibration damping function of the sensor bracket structure and the noise filtering function of the sensor signal conditioning module. The structure of the proposed monitoring system is shown in Figure 1.
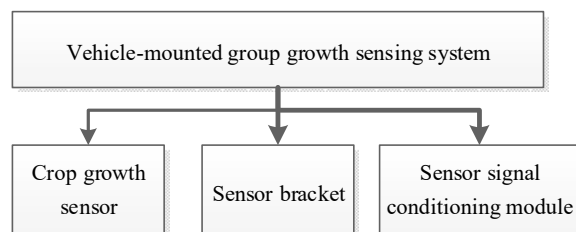
Figure 1. Structure of vehicle-mounted crop growth monitoring system.

2.1. Vehicle-Mounted Crop Growth Sensor

The multispectral crop growth sensor of the proposed monitoring system is the CGMD302 multispectral crop growth sensor (as shown in Figure 2) developed by Nanjing Agricultural University [38,39]. Its key specifications are monitoring wavelength bands: 730 nm and 815 nm; field of view angle: 27°; working height: 1.0–1.5 m above the crop canopy.
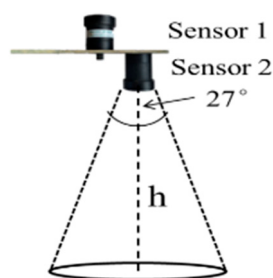
Figure 2. Measurement principle of the CGMD302 multispectral crop growth sensor.

2.2. Design of Sensor Signal Conditioning Module

2.2.1. Design of Sensor Signal Amplification and Filtering Buffer Circuit

Considering that the CGMD302 multispectral crop growth sensor outputs a weak current signal of the order of nA, we made use of the two cores of the AD8032 single-power supply voltage dual-core feedback amplifier produced by Analog Devices to design a T-type resistance feedback network amplification circuit and a Sallen–Key filter circuit (configured as an operational amplifier working in voltage following mode), thus forming the amplification and filtering buffer circuit for processing the sensor signal, as shown in Figure 3. The purpose of the parallel-connection voltage-stabilizing capacitors at the inlet and outlet of the signal amplification and filtering buffer circuit of the multispectral crop growth sensor is to improve the stability and anti-interference ability of the circuit. The key specifications of the AD8032 are input bias current: 0.45 μA, input offset voltage: 1 μV, and total harmonic distortion (THD): −62 dBc.
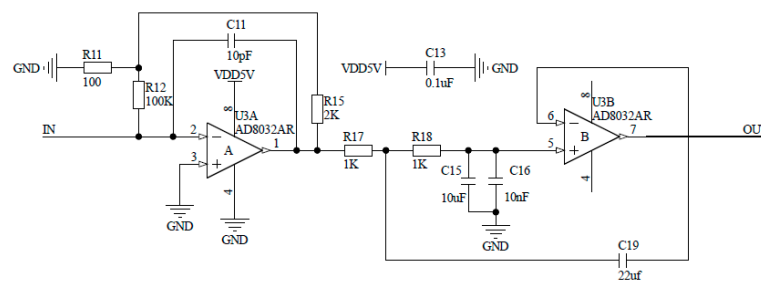

Figure 3. Sensor signal amplification and filtering buffer circuit.

2.2.2. Design of Programmable Filter Based on LTC1064

The original signal of the multispectral crop growth sensor still contains low-frequency noise signals after being processed by the front filtering buffer circuit. Some noise signals of different frequencies will be mixed with the original signal in the process of I-V conversion and amplification performed in the front stage. Therefore, it is necessary to filter the signal once again in the rear-stage circuit so as to improve the accuracy of the acquired signal. In the process of designing a conventional filter, the cut-off frequency is set at first, and then the filter parameters are solved. The filters designed using this design method mostly have low accuracy, and their cut-off frequency cannot be changed. Because of these deficiencies, we designed a program-controlled filter circuit based on the LTC1064-3 filter produced by Analog Devices, as shown in Figure 4. A PWM signal with a duty cycle of 50% is generated through proper settings of the frequency division coefficient and automatic reloading coefficient of the general-purpose timer in the STM32429ZET6 chip, and the PWM signal is passed to pin 11 of the LTC1064-3 chip to provide the clock signal of the filter. The cut-off frequency of the LTC1064-3 filter is set to 5 Hz to enable the generation of the 750 Hz PWM signal.
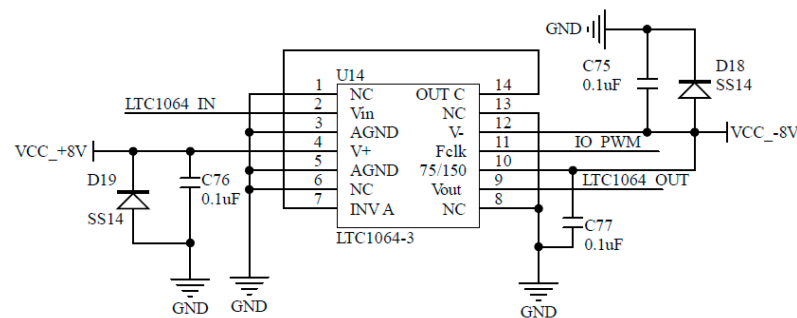

Figure 4. Bessel programmable low-pass filter.

2.3. Design and Performance Simulation of Sensor Bracket Based on FEM

2.3.1. Design of Sensor Bracket and Establishment of Finite Element Model

To overcome the impact of vibration of agricultural machinery on the sensing accuracy and performance of crop growth sensors, we designed a truss-type sensor bracket based on the principles that can be used to improve the dynamic characteristic parameters and vibration parameters of the sensor bracket. Considering that the support system is a long cantilever beam, it is necessary to enhance the overall structural stiffness. Based on experience, we chose a reinforced triangular structure. The rods used to make the plane truss of the new sensor bracket have a rectangular cross-section; that is, they are made of square steel. The truss adopts a trapezoidal structure. The web members are arranged in the fully inclined form, with an inclination angle of 45°. The steel material used to make the sensor bracket is Q235 steel. Its specifications are as follows: Poisson's ratio: 0.3; elastic modulus: 2.068 × 105 Mpa, material density: 7850 kg/m^3, tensile strength: 375–460 MPa, yield limit: 235 MPa, and allowable stress: 117.5 MPa. The new sensor bracket has a length of 4 m, and its allowable bending is 4000 × (2/500) = 16 mm. The structure of the truss-type sensor bracket is shown in Figure 5.
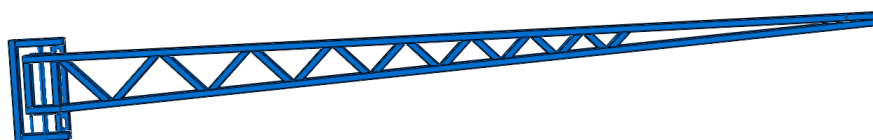
Figure 5. Structure of truss-type sensor bracket.

We built a 3D geometric model of the new sensor bracket and its assembly model in the Pro/E 2016 3D parametric modeling software, according to the actual size and assembly relationship of the sensor bracket, and then generated an .stp file and imported it into the finite element analysis software ABAQUS 6.10 for finite element simulation analysis. In the process of establishing the finite element model, the non-connecting components, chamfering, welding sites, and circular angles in the geometric model of the sensor bracket were simplified, so as to reduce the calculation workload of the geometric model as much as possible while ensuring the calculation accuracy of the strength and dynamic response of the main structure of the new sensor bracket. The established finite element model retains the main structure and key components of the sensor bracket as well as the connection relationship between them. In addition, the model is loaded with reasonable and effective constraints and loads [40,41].

2.3.2. Finite Element Modal Simulation of the Sensor Bracket

The theoretical basis of modal analysis is the vibration theory of the elastic body. The basic equation of typical damp-free modal analysis is the classical eigenvalue solution problem. The dynamic balance equation for the structure without damping is:

$$\left(-\omega^2[M]\{\varnothing\} + [K]\{\varnothing\}\right)e^{i\omega t} = 0 \tag{1}$$

where $[M]$ is the mass matrix of the structure system, which is composed of the mass matrices of all units; $[K]$ is the stiffness matrix of the structure system; $\{\varnothing\}$ is the system modal vector matrix; and ω is the natural frequency.

The eigenvalue solution equation is:

$$\left([K] - \omega^2[M]\right)\{\varnothing\} = 0 \tag{2}$$

The necessary and sufficient condition for the existence of a non-zero solution in Equation (2) is a determinant

$$\left|[K] - \omega^2[M]\right| = 0 \tag{3}$$

In this study, the Lanczos solution method of ABAQUS/standard implicit analysis solver was used to analyze and extract the structural modes of a conventional cantilever bracket and the proposed truss-type sensor bracket.

2.3.3. Finite Element Dynamic Simulation of the Sensor Bracket

To verify the ability of the new sensor bracket to overcome the impact of vibration when the agricultural machine is moving in the field, we conducted a dynamic simulation of the new sensor bracket using the finite element analysis method for nonlinear mechanical structures. The dynamic equation used in the nonlinear dynamic analysis is:

$$M\ddot{d}(t) + C\dot{d}(t) + f^{\text{int}}(t) = Q(t) \tag{4}$$

where M is the mass matrix of the sensor bracket, C is the damping matrix of the sensor bracket, $Q(t)$ is the node load vector, $f^{\text{int}}(t)$ is the internal force vector of the sensor bracket, and $\dot{d}(t)$ and $\ddot{d}(t)$ represent the velocity and acceleration of the structure, respectively.

The finite element discrete dynamic equation of nonlinear mechanical structure at the moment of $t = t^{n+1}$ is established using the Newmark implicit integration method, which is:

$$r(d^{n+1}, t^{n+1}) = M\ddot{d}^{n+1} + f^{\text{int}}(d^{n+1}, t^{n+1}) - f^{ext}(d^{n+1}, t^{n+1}) \tag{5}$$

where $r(d^{n+1}, t^{n+1})$ is the residual column matrix; $f^{ext}(d^{n+1}, t^{n+1})$ is the external force matrix of the sensor bracket; and $d^{n+1}, \dot{d}^{n+1}$, and $\ddot{d}^{n+1}$ represent the displacement, velocity, and acceleration array of the structure, respectively.

The theoretical basis of the implicit integration method is the assumption that the acceleration changes linearly within the time interval Δt, and the formulas for calculating displacement d^{n+1} and velocity $\dot{d}^{n+1}$ are as follows:

$$d^{n+1} = \tilde{d}^{n+1} + \beta(\Delta t^n)^2 \ddot{d}^{n+1} \tag{6}$$

$$\dot{d}^{n+1} = \dot{\tilde{d}}^{n+1} + \gamma \Delta t^n \tilde{d}^{n+1} \tag{7}$$

where β and γ are parameters that can be adjusted according to the requirements on integration accuracy and stability; $\tilde{d}^{n+1}$ and $\dot{\tilde{d}}^{n+1}$ are as follows:

$$\tilde{d}^{n+1} = d^n + \Delta t^n \dot{d}^n + (\Delta t^n)^2 / 2 (1 - 2\beta) \ddot{d}^n \tag{8}$$

$$\dot{\tilde{d}}^{n+1} = \dot{d}^n + (1 - \gamma) \Delta t^n \ddot{\tilde{d}}^n \tag{9}$$

The formula for calculating acceleration in the time interval Δt can be obtained by solving Equation (9):

$$\ddot{d}^{n+1} = \frac{1}{\beta(\Delta t^n)^2} (d^{n+1} - \tilde{d}^{n+1}) \text{ when } \beta > 0 \tag{10}$$

The formula for calculating the value in the assumed time interval Δt using the α method is:

$$d^{n+\alpha} = (1 + \alpha)d^{n+1} - \alpha d^n \tag{11}$$

The internal force vector is defined as $f^{\text{int}} = Kd^{n+\alpha} = (1 + \alpha)Kd^{n+1} - \alpha Kd^n$. α is the parameter that can be adjusted according to the requirement on high-frequency numerical dissipation.

Updating Equation (5) using the α method, we can obtain the nonlinear algebraic equation:

$$r(d^{n+1}, t^{n+1}) = M\ddot{d}^{n+1} + f^{\text{int}}(d^{n+\alpha}, t^{n+1}) - f^{ext}(d^{n+\alpha}, t^{n+1}) \tag{12}$$

Substituting the acceleration formula (10) in the time interval Δt into Equation (12), we can get

$$r(d^{n+1}, t^{n+1}) = \frac{1}{\beta(\Delta t)^2} M(d^{n+1} - \tilde{d}^{n+1}) + f^{\text{int}}(d^{n+\alpha}, t^{n+1}) - f^{ext}(d^{n+\alpha}, t^{n+1}) \tag{13}$$

Using the Newton–Raphson iterative method to calculate the nonlinear dynamic equation in the ABAQUS software, we simulated the dynamic response of the new sensor bracket.

2.4. Design of Experiment

2.4.1. Vibration Testing of Agricultural Machinery and Sensor Bracket

To verify the simulation accuracy of the finite element model and ascertain the frequencies of the excitation a typical agricultural machine exerts on the sensor bracket in the driving direction, transverse direction, and vertical direction, we conducted an experiment to investigate the dynamic vibration response characteristics of an agricultural machine and a conventional cantilever bracket in the Rugao Test and Demonstration Base of Nanjing Agricultural University in July 2023. In the experiment, a 356A33 micro piezoelectric triaxial acceleration sensor supplied by PCB Piezotronics Inc. (Depew, NY, USA) was used to acquire in real time the vibration frequency and vibration amplitude signals of the experimental agricultural machine and conventional cantilever bracket. Its key specifications are as follows: the frequency acquisition range of the x-axis is 2–7000 hz and the accuracy is ±5%. The frequency acquisition range of the y-axis and z-axis is 2–10,000 hz, and the accuracy is ±5%. The vibration analyzer used in the experiment was the DH5981 8-channel distributed dynamic signal test and analysis system produced by Jangsu Donghua Testing Technology Co., Ltd (Taizhou, China). Its key specifications are as follows: the sampling frequency is 128 kHz, and the A/D conversion resolution is 24-bit.

Eight micro piezoelectric triaxial acceleration sensors were fixed to the assembly frame (used for fixing the sensor bracket to the experimental agricultural machine) of the experimental agricultural machine and different positions of the conventional cantilever bracket were used to measure the vibration frequency and vibration amplitude of the experimental agricultural machine as a single excitation source as well as the vibration frequency and vibration amplitude values at different positions of the conventional cantilever bracket. The specific installation positions are shown in Figure 6 and Table 1. The engine of the experimental agricultural machine was working during the test.
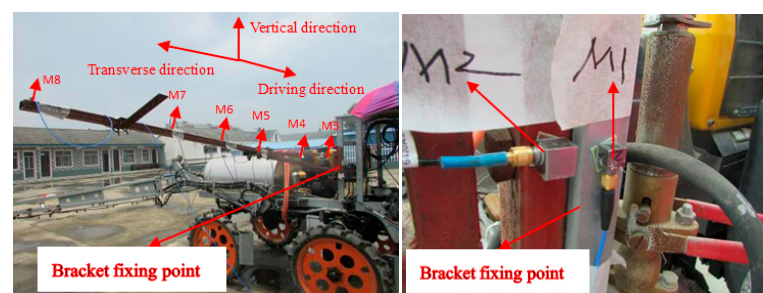

Figure 6. Installation location of three-axis accelerometer.

Table 1. The distances of the sensors from the fixing point.

Sensor Number	M1	M2	M3	M4	M5	M6	M7	M8
Distance/cm	0	2	74	122	179.5	207	245	299

2.4.2. Experiment of Testing Sensing Performance of Crop Growth Sensor under Vibration Condition

We conducted an experiment to test the impact of vibration of the sensor bracket on the sensing performance of vehicle-mounted crop growth sensors in the Rugao Test and Demonstration Base of Nanjing Agricultural University from May to September 2023. As shown in Figure 7, the agricultural machinery platform selected for the experiment was a 3WPZG-800 self-propelled, high-clearance bar-type spray vehicle produced by Fengzhao Hangtai (Nanjing, China) Mechanization Co., Ltd. (Nanjing, China). The vehicle-mounted crop growth sensors used in the experiment were CGMD302 multispectral sensors (spectral bands: 730 nm and 815 nm), the TOPCON CropSpec active light source sensor (spectral bands: 735 nm and 808 nm), and the GreenSeeker RT 200 active light source sensor (spectral bands: 656 nm and 774 nm). The experiment site was planted with two varieties of rice, namely Huaidao 5 and Wuyungeng 27. Three nitrogen levels were used in the experiment: 0, 150, and 300 kg/ha; the ratio of base fertilizer/tiller fertilizer/flower-promoting fertilizer/flower-preserving fertilizer was 4:2:2; and two density settings (row spacing × plant spacing) were used: 30 cm × 15 cm and 50 cm × 15 cm. The experiment site was partitioned into 36 plots with a size of 5 m × 6 m, and the plots were treated with 12 kinds of treatments (every three plots were treated with the same treatment). The positions of the plots were chosen randomly. The effects of the vibration of the spray vehicle itself and the vibrations generated at different operating speeds (1.5, 3, and 4.5 km/h) on the sensing performance of the vehicle-mounted sensor were tested, and the performance levels of different sensors in acquiring agronomic parameters were compared.


Figure 7. Test platform of sensors.

3. Results

3.1. Verification of Simulation Accuracy of Finite Element Model of the Sensor Bracket

To verify the accuracy of the finite element simulation results of the sensor bracket, we compared and analyzed the time domain response curves of acceleration in three directions of the bracket tail end (M8) based on the data of vibration testing and finite element simulation. It can be seen from Figure 8 that the period and amplitude values obtained through simulation are basically consistent with the values obtained through vibration testing; the values of the maximum and average relative errors of their amplitude are shown in Table 2. In the vertical, driving, and transverse directions, the maximum relative errors are 0.22%, 0.16%, and 0.92%, respectively, and the average relative errors are 0.06%, 0.15%, and 0.32%, respectively. This indicates that the finite element model of the sensor bracket established in this study has good simulation accuracy.

(a)

(b)

(c)
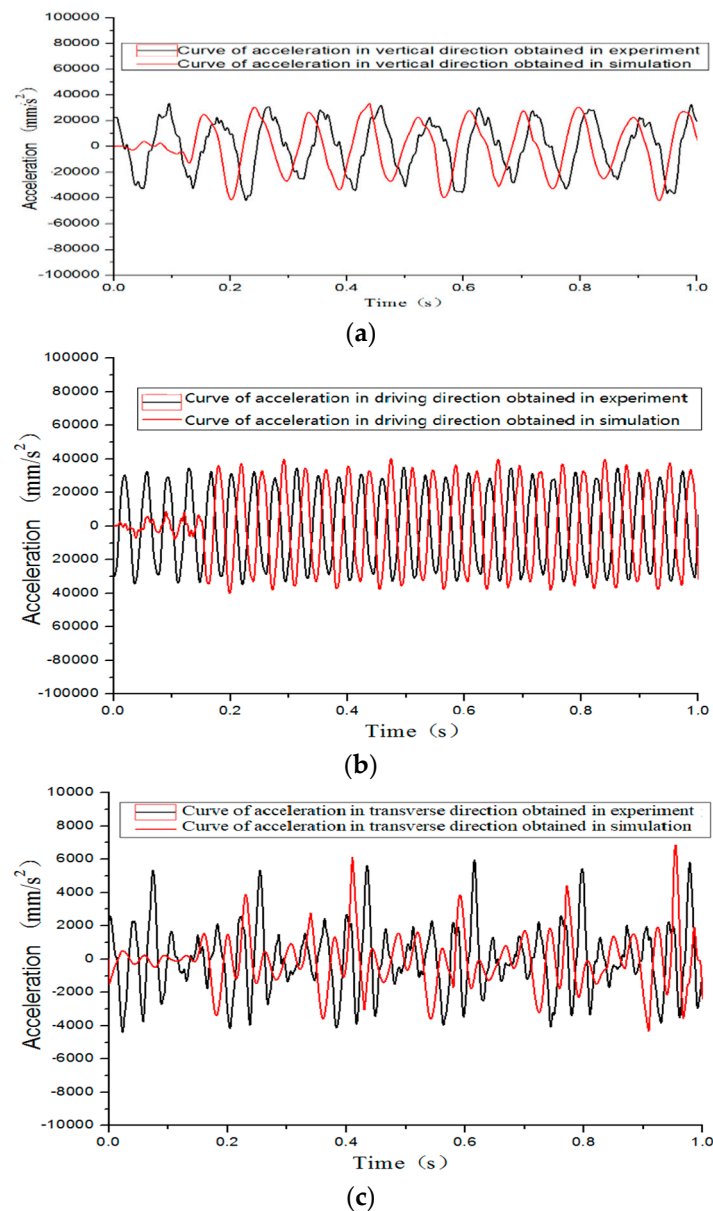
Figure 8. Comparison of simulation and test results at 8 locations. (**a**) Curves of vertical acceleration response. (**b**) Curves of acceleration response in driving direction. (**c**) Curves of lateral acceleration response.

Table 2. The relative errors of simulated and experimental acceleration curves.

Direction	Vertical	Driving	Transverse
Maximum relative error	0.22%	0.16%	0.92%
Average relative error	0.06%	0.15%	0.32%

3.2. Analysis of Self-Vibration Damping Performance of Truss-Type Sensor Bracket

3.2.1. Modal Analysis of Sensor Bracket

When an agricultural machine is traveling, the resonance frequencies of the sensor bracket are mostly in the low-order range. Therefore, we extracted the first eight natural frequencies of the cantilever bracket and truss-type sensor bracket for comparative analysis. It can be seen from Table 3 that the first eight natural frequencies of truss-type sensor bracket obtained by finite element modal analysis are far from the key excitation frequencies of the spray vehicle, such as 28.564 Hz, 34.18 Hz, 17.09 Hz, and 11.475 Hz. There is a step increase

from the third-order natural frequency of the truss-type sensor bracket to the fourth-order natural frequency, indicating that the truss-type sensor bracket can evade the key excitation frequencies of the spray vehicle better than the cantilever bracket. The comparison results of vibration modes of the cantilever bracket and truss-type sensor bracket show that the vibration mode of the truss-type sensor bracket obtained through finite element modal analysis is better than that of the cantilever bracket. The stability of the truss-type sensor bracket is even better in the high-order range (as shown in Figure 9).

**Table 3.** First 8 natural frequencies of new bracket system.

Order	1	2	3	4	5	6	7	8
Natural frequencies of cantilever/Hz	7.5849	9.1734	32.042	36.817	58.016	97.480	117.02	123.51
Natural frequencies of truss/Hz	2.9860	8.6907	22.464	61.709	76.384	114.18	133.81	151.40

(**a**)

(**b**)
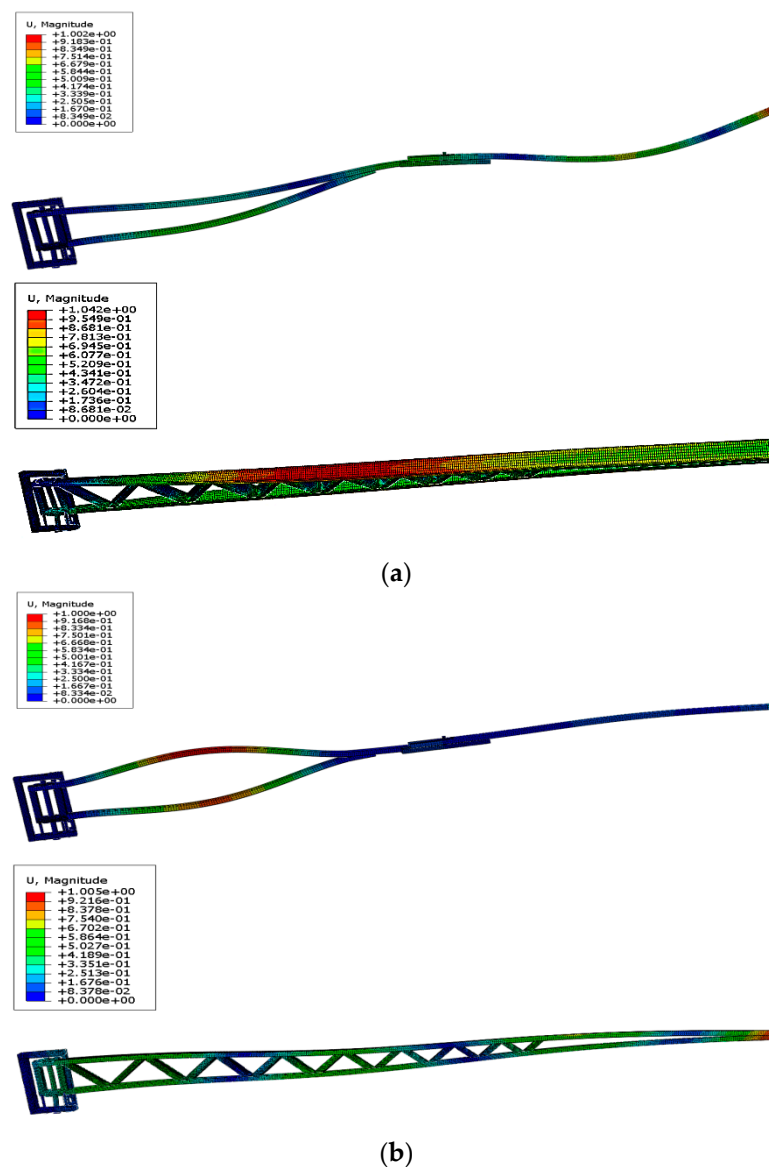
Figure 9. Comparison of main vibration modes between truss-type and cantilever bracket. (**a**) Comparison of 7th order vibration modes. (**b**) Comparison of 8th order vibration modes.

3.2.2. Dynamic Simulation of the Sensor Bracket

Figure 10 shows the curves of the acceleration response (three directions) at the far end of the truss-type sensor bracket and the cantilever sensor bracket, obtained through finite element simulation. The curves indicate: (1) the acceleration responses of the two sensor brackets have roughly the same periodicity; (2) while there is only a small amplitude difference between the acceleration responses of the two sensor brackets in the vertical direction, the acceleration amplitude of the truss-type sensor bracket is significantly smaller than that of the cantilever sensor bracket in the driving and transverse directions, which proves that the proposed truss-type sensor bracket can damp vibration effectively.


(a)

(b)

(c)
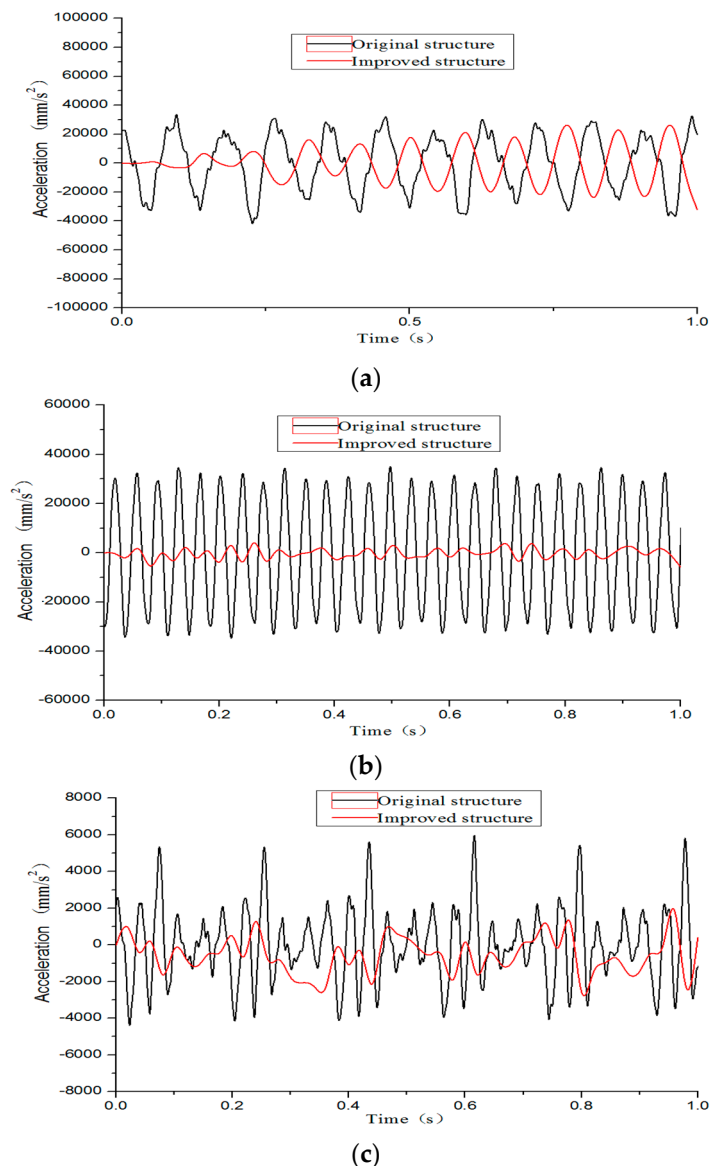
Figure 10. Comparison of the acceleration response between truss-type sensor bracket and cantilever bracket. (**a**) Vertical direction. (**b**) Driving direction. (**c**) Transverse direction.

3.3. Analysis of Sensing Performance of Crop Growth Sensors under the Condition of Vibration

3.3.1. Analysis of the Impact of Stationary Vibration on the Performance of the Vehicle-Mounted Sensor in Detecting Spectral Reflectance

The variation curves of spectral reflectance plotted according to the data acquired by the spectral sensor at two different wavelength bands in the experiment conducted to investigate the impact of stationary vibration on the performance of the vehicle-mounted

sensor in measuring spectral reflectance are shown in Figure 11. The values of average, variance, and CV corresponding to the 815 nm and 730 nm wavelength bands are shown in Table 4. It can be seen from the figure and table that the reflectance curves obtained at the 815 nm and 730 nm wavelength bands when the spray vehicle Is stationary are roughly consistent with their counterparts obtained when the spray vehicle is moving. At the wavelength band of 815 nm, the differences between the values of average, variance, and coefficient obtained under the condition of stationary vibration and those obtained under the condition of in-travel vibration are 0.24%, 0.03%, and 0.07%, respectively; the differences are 0.26%, 0.01%, and 0.03%, respectively, at the wavelength band of 730 nm.
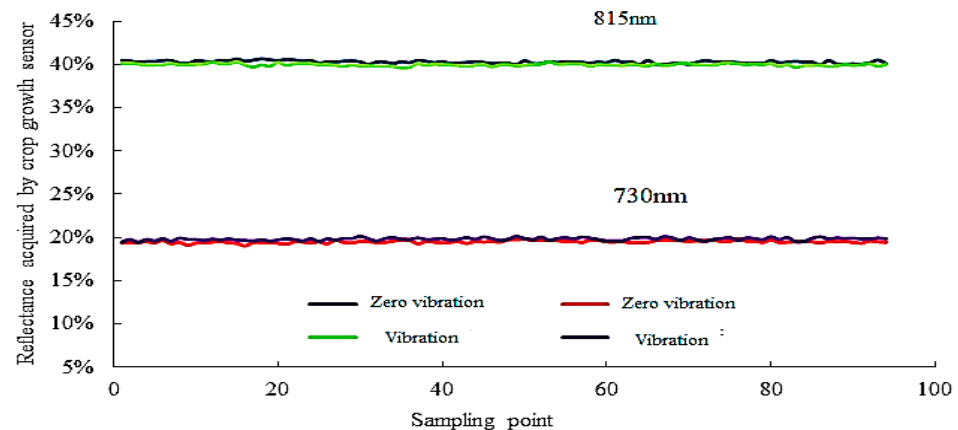

Figure 11. Changes in measured light reflectance under the influence of vibration.

Table 4. Variation of light reflectance under the impact of vibration.

State	Wavelength	Mean	Var	CV
Stationary		40.20%	0.16%	0.41%
Vibration	815 nm	39.96%	0.13%	0.34%
Difference		0.24%	0.03%	0.07%
Stationary		19.55%	0.15%	0.75%
Vibration	730 nm	19.81%	0.15%	0.78%
Difference		0.26%	0.01%	0.03%

3.3.2. Analysis of the Impact of Vibration on the Monitoring Performance of Vehicle-Mounted Sensors under Different Traveling Speeds

The variation curves of rice canopy NDRE were plotted according to the data acquired by the vehicle-mounted crop growth sensor in different crop growth stages under different traveling speeds in the experiment conducted to investigate the impact of in-travel vibration on the performance of the vehicle-mounted sensor in measuring spectral reflectance are shown in Figure 12. It can be seen from the figure that the values of significant difference P of rice canopy NDRE obtained under three traveling speeds are 0.454, 0.703, 0.810, and 0.838, respectively, for the four growth stages; the Cvmax values are 8.3%, 4.6%, 3.7%, and 3.6%, respectively, for the four growth stages; and the RMSEmax values are 0.008, 0.007, 0.007, and 0.008, respectively, for the four growth stages. The experimental results show that the vehicle-mounted crop growth monitoring system proposed in this paper can significantly mitigate the impact of vibration of agricultural machinery on the monitoring performance of the vehicle-mounted crop growth sensor, and the monitoring performance of the vehicle-mounted crop growth sensor is quite stable.
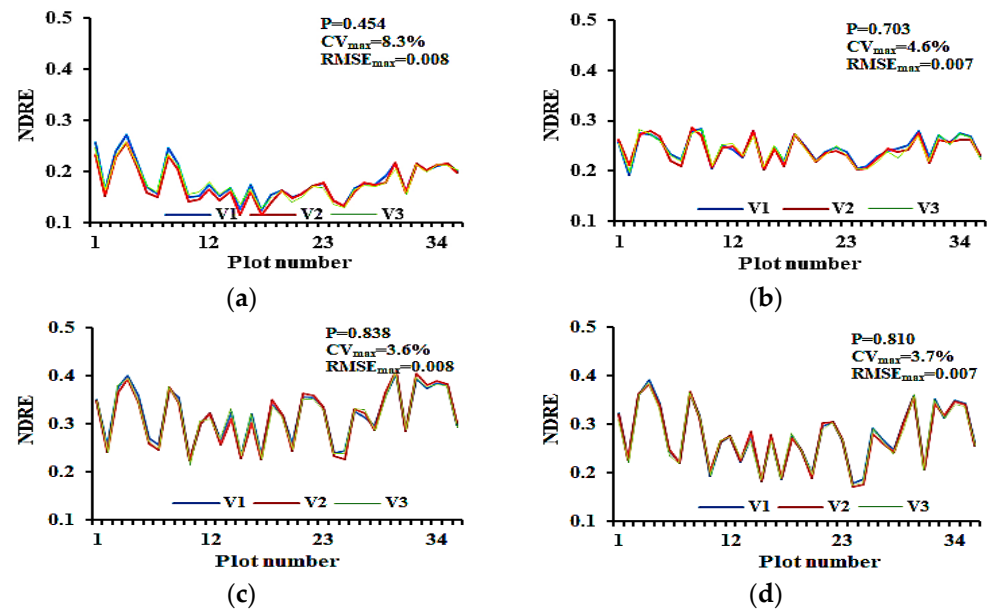
Figure 12. NDRE values acquired at different speeds of CGMD in different growth stages. (**a**) Tillering stage. (**b**) Jointing stage. (**c**) Booting stage. (**d**) Heading stage.

3.3.3. Comparative Analysis of Monitoring Performance of Different Sensors in Monitoring Agronomic Parameters

Considering that the NDRE values acquired by the GreenSeeker sensor in the booting and heading stages of rice crops tend to saturate, we compared and analyzed the fitting results of the NDRE values acquired by different sensors in the tillering, jointing, and tillering and jointing stages of the rice crop and the plant nitrogen uptake (PNU) values of the rice crop in the corresponding growth stages. As can be seen from Figure 13, the R2 values obtained by the CGMD, CropSpec, and GreenSeeker sensors in the tillering stage are 0.8757, 0.7781, and 0.6822, respectively, and the RMSE values are 0.7157, 0.9564, and 1.1445, respectively; the R2 values in the jointing stage are 0.7194, 0.43, and 0.5863, respectively, and the RMSE values are 2.2341, 3.1843, and 2.7127, respectively; the R2 values in the tillering and jointing stage are 0.795, 0.6882, and 0.6467, respectively, and the RMSE values are 2.0952, 2.5841, and 2.7506, respectively. The results show that the proposed crop growth monitoring system can accurately monitor the growth of rice.
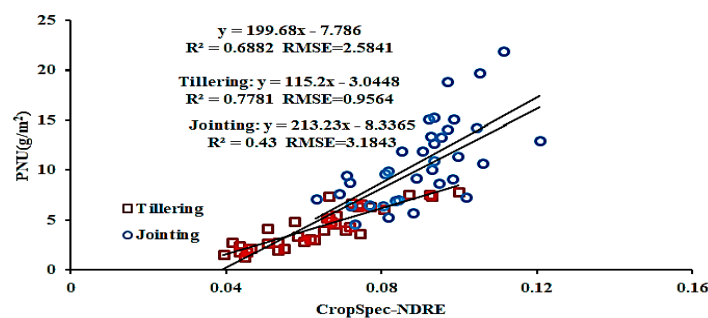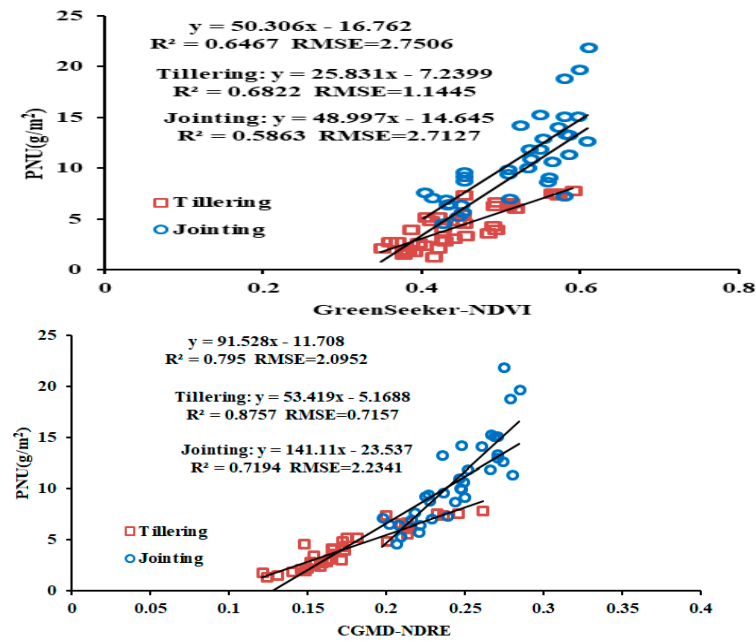

Figure 13. *Cont*.

Figure 13. Relationship between NDRE obtained by different sensors and agronomic parameters.

4. Discussion

4.1. Analysis of the Design and Performance of Vehicle-Mounted Crop Growth Monitoring System

At present, the existing vehicle-mounted crop growth sensors are normally fixed directly on the cantilever beam extended from the carrier agricultural machine. The crop growth monitoring is performed when the carrier agricultural machine is idle [42–44], so the impact of vibration of agricultural machinery on the monitoring performance and accuracy of the vehicle-mounted crop growth sensor is not considered. Because of this deficiency, we designed a truss-type sensor bracket, established a finite element structural dynamic model of the system structure of the new vehicle-mounted sensor bracket using the ABAQUS finite element analysis software, and analyzed the performance of the sensor bracket structure through modal and dynamic analysis as well as a vibration testing experiment. The modal simulation results show that the truss -type sensor bracket can evade the key excitation frequencies of agricultural machinery better than the cantilever bracket structure, and the first eight vibration modes of the truss-type sensor bracket are better than those of the cantilever bracket (its stability is even better in the high-order range). As indicated by the results of dynamic simulation analysis, the acceleration responses of the two bracket systems have basically the same periodicity. The acceleration amplitude of the truss-type sensor bracket is significantly smaller than that of the cantilever sensor bracket in the driving and transverse directions, which proves that the truss-type sensor bracket can damp vibration effectively.

As indicated by the results of the experiment conducted to investigate the impact of stationary vibration on the performance of the vehicle-mounted sensor in measuring spectral reflectance, the designed sensor signal conditioning circuit can effectively eliminate the interference of noise signal, which is reflected by the smallness of the difference between the maximum CV (which is 0.75%) of the spectral reflectance values acquired under the condition of zero vibration and the maximum CV (which is 0.78%) of the spectral reflectance values acquired under the condition of stationary vibration. As can be derived from the results of the experiment conducted to investigate the impact of in-travel vibration on the performance of the vehicle-mounted sensor in measuring spectral reflectance in different growth stages, the values of significant difference P of rice canopy NDRE obtained under different traveling speeds are 0.454, 0.703, 0.810, and 0.838, respectively, for the four growth stages. The experimental results show that the proposed vehicle-mounted crop

growth monitoring system can significantly mitigate the impact of vibration of agricultural machinery on the detection performance of vehicle-mounted crop growth sensors.

The proposed monitoring system exhibits good monitoring accuracy and stability when the carrier agricultural machine is vibrating. However, we adopted the trial-and-error method to design a new sensor bracket based on the results of finite element simulation analysis and past experience, which requires a lengthy period and presents high requirements on the expertise of the designers. Therefore, it is necessary to explore the optimal design methods for sensor brackets in future research, such as the topology optimization method, so that their vibration can be constrained or minimized. In addition, the proposed vehicle-mounted monitoring system is quite heavy because the sensor bracket is made of structural steel. Therefore, there is a need to explore lighter materials suitable for making sensor brackets.

4.2. PNU Estimation Using Different Vehicle-Mounted Sensors

Plant nitrogen uptake (PNU) refers to the nitrogen accumulation per unit area. It comprehensively reflects the nitrogen nutrition status and growth quality of the plants and also provides an important basis for nitrogen application in the middle and late stages. Some scholars have conducted experiments to monitor rice PNU using the handheld GreenSeeker sensor, proving that the measured canopy NDVI is significantly correlated with rice PNU [45–47]. Both the CGMD sensor and the CropSpec sensor can be used to monitor the NDRE level of the crop canopy. CGMD can measure spectral reflectance at wavelength bands of 730 nm and 815 nm, while CropSpec can measure spectral reflectance at wavelength bands of 735 nm and 808 nm.

The results of this study show that the PNU estimation accuracy levels of CGMD and CropSpec are higher than that of GreenSeeker, which agrees with the research results of Yu et al. [48] and Cordero et al. [49]. The fact that the PNU estimation accuracy of CGMD is better than that of CropSpec also indicates that the proposed crop growth monitoring system can significantly reduce the impact of vibration of agricultural machinery on the detection performance of vehicle-mounted crop growth sensors.

5. Conclusions

This study developed a vehicle-mounted crop growth monitoring system with vibration suppression capability. The system consists of a crop growth sensor, truss-type sensor bracket, and sensor signal conditioning module. In an experiment conducted to test the performance of the proposed monitoring system under different traveling speeds in different crop growth stages, the values of significant difference P of rice canopy NDRE obtained under different traveling speeds were 0.454, 0.703, 0.810, and 0.838, respectively, for the four growth stages; the CVmax values were 8.3%, 4.6%, 3.7%, and 3.6%, respectively, for the four growth stages; and the RMSEmax values were 0.008, 0.007, 0.007, and 0.008, respectively, for the four growth stages. In an experiment conducted to compare the performance levels of different vehicle-mounted sensors, the proposed monitoring system achieved the highest performance in PNU prediction, yielding R^2 values of 0.8757, 0.7194, and 0.795, respectively, and RMSE values of 0.7157, 2.2341, and 2.0952, respectively, in the tillering stage, jointing stage, and tillering and jointing stage.

Author Contributions: Conceptualization, S.Y. and W.C.; methodology, S.Y., W.C. and Q.C.; software, S.Y. and J.N.; validation, S.Y., W.C., Y.T. and Y.Z.; formal analysis, S.Y., W.C. and X.L.; investigation, W.Z.; resources, W.C.; data curation, S.Y. and X.L.; writing—original draft preparation, S.Y.; writing—review and editing, S.Y., W.C., X.L. and J.N. All authors have read and agreed to the published version of the manuscript.

Data Availability Statement: The data presented in this study are available on request from the corresponding author.

Conflicts of Interest: The authors declare no conflicts of interest.

References

1. He, G.; Liu, X.; Cui, Z. Achieving global food security by focusing on nitrogen efficiency potentials and local production. *Glob. Food Secur.* **2021**, *29*, 100536. [CrossRef]
2. Shah, F.; Wu, W. Soil and Crop Management Strategies to Ensure Higher Crop Productivity within Sustainable Environments. *Sustainability* **2019**, *11*, 1485. [CrossRef]
3. Ma, K.; Diao, G. Research on the contribution rate of fertilizer to grain yield in China. *J. Plant Nutr. Fertil.* **2018**, *24*, 1113–1120. [CrossRef]
4. Obour, A.K.; Mikha, M.M.; Holman, J.D.; Stahlman, P.W. Changes in soil surface chemistry after fifty years of tillage and nitrogen fertilization. *Geoderma* **2017**, *308*, 46–53. [CrossRef]
5. Fu, H.; Li, N.; Cheng, Q.; Liao, Q.; Nie, J.; Yin, H.; Shu, C.; Li, L.; Wang, Z.; Sun, Y.; et al. Energy, environmental, and economic benefits of integrated paddy field farming. *Energy* **2024**, *297*, 131251. [CrossRef]
6. Guerrero, A.; Mouazen, A.M. Evaluation of variable rate nitrogen fertilization scenarios in cereal crops from economic, environmental and technical perspective. *Soil Tillage Res.* **2021**, *213*, 105110. [CrossRef]
7. Guerrero, A.; Neve, S.D.; Mouazen, A.M. Data fusion approach for map-based variable-rate nitrogen fertilization in barley and wheat. *Soil Tillage Res.* **2021**, *205*, 104789. [CrossRef]
8. Cao, W. *Digital Farming Technology*; Science Press: Beijing, China, 2008.
9. Balafoutis, A.; Beck, B.; Fountas, S.; Vangeyte, J.; Wal, T.V.d.; Soto, I.; Gómez-Barbero, M.; Barnes, A.; Eory, V. Precision Agriculture Technologies Positively Contributing to GHG Emissions Mitigation, Farm Productivity and Economics. *Sustainability* **2017**, *9*, 1339. [CrossRef]
10. Munnaf, M.A.; Haesaert, G.; Meirvenne, M.V.; Mouazen, A.M. Chapter Five—Site-specific seeding using multi-sensor and data fusion techniques: A review. *Adv. Agron.* **2020**, *161*, 241–323. [CrossRef]
11. Munnaf, M.A.; Haesaert, G.; Meirvenne, M.V.; Mouazen, A.M. Map-based site-specific seeding of consumption potato production using high-resolution soil and crop data fusion. *Comput. Electron. Agric.* **2020**, *178*, 105752. [CrossRef]
12. Munnaf, M.A.; Haesaert, G.; Mouazen, A.M. Site-specific seeding for maize production using management zone maps delineated with multi-sensors data fusion scheme. *Soil Tillage Res.* **2022**, *220*, 105377. [CrossRef]
13. Munnaf, M.A.; Haesaert, G.; Mouazen, A.M. Map-based site-specific seeding of seed potato production by fusion of proximal and remote sensing data. *Soil Tillage Res.* **2021**, *206*, 104801. [CrossRef]
14. Lundström, C.; Lindblom, J. Considering farmers' situated knowledge of using agricultural decision support systems (AgriDSS) to Foster farming practices: The case of CropSAT. *Agric. Syst.* **2018**, *159*, 9–20. [CrossRef]
15. Thompson, A.L.; Conrad, A.; Conley, M.M.; Shrock, H.; Taft, B.; Miksch, C.; Mills, T.; Dyer, J.M. Professor: A motorized field-based phenotyping cart. *HardwareX* **2018**, *4*, e00025. [CrossRef]
16. Stone, M.L.; Solie, J.B.; Raun, W.R.; Whitney, R.W.; Taylor, S.L.; Ringer, J.D. Use of spectral radiance for correcting in-season fertilizer nitrogen deficiencies in winter wheat. *Trans. ASAE* **1996**, *39*, 1623–1631. [CrossRef]
17. Link, A.; Panitzki, M.; Reusch, S.; Robert, P.C. Hydro N-sensor: Tractormounted remote sensing for variable nitrogen fertilization. In Proceedings of the 6th International Conference on Precision Agriculture & Other Precision Resources Management, Minneapolis, MN, USA, 14–17 July 2002.
18. Holland, K.H.; Schepers, J.S.; Shanahan, J.F. Plant canopy sensor with modulated polychromatic light source. In Proceedings of the International Conference on Precision Agriculture and Other Precision Resources Management, Minneapolis, MN, USA, 25–28 July 2004.
19. David, J.M. Twenty five years of remote sensing in precision agriculture: Key advances and remaining knowledge gaps. *Biosyst. Eng.* **2013**, *114*, 358–371. [CrossRef]
20. Scharf, P.C.; Shannon, D.K.; Palm, H.L.; Sudduth, K.A.; Drummond, S.T.; Kitchen, N.R.; Mueller, L.J.; Hubbard, V.C.; Oliveira, L.F. Sensor-Based Nitrogen Applications Out-Performed Producer-Chosen Rates for Corn in On-Farm Demonstrations. *Agron. J.* **2011**, *103*, 1683–1691. [CrossRef]
21. Pallottino, F.; Antonucci, F.; Costa, C.; Bisaglia, C.; Figorilli, S.; Menesatti, P. Optoelectronic proximal sensing vehicle-mounted technologies in precision agriculture: A review. *Comput. Electron. Agric.* **2019**, *162*, 859–873. [CrossRef]
22. Temmerman, J.D.; Deprez, K.; Anthonis, J.; Ramon, H. Conceptual Cab Suspension System for a Self-propelled Agricultural Machine, Part 1: Development of a Linear Mathematical Model. *Biosyst. Eng.* **2004**, *89*, 409–416. [CrossRef]
23. Kang, T.H.; Kaizu, Y. Vibration analysis during grass harvesting according to ISO vibration standards. *Comput. Electron. Agric.* **2011**, *79*, 226–235. [CrossRef]
24. Filippi, M.; Carrera, E.; Zenkour, A.M. Static analyses of FGM beams by various theories and finite elements. *Compos. Part B Eng.* **2015**, *72*, 1–9. [CrossRef]
25. David, S.A.; Sousa, R.V.; Valentim, C.A.; Tabile, R.A.; Machado, J.A. Fractional PID controller in an active image stabilization system for mitigating vibration effects in agricultural tractors. *Comput. Electron. Agric.* **2016**, *131*, 1–9. [CrossRef]
26. Mohammadikia, R.; Aliasghary, M. Design of an interval type-2 fractional order fuzzy controller for a tractor active suspension system. *Comput. Electron. Agric.* **2019**, *167*, 105049. [CrossRef]

27. Katili, I.; Syahril, T.; Katili, A.M. Static and free vibration analysis of FGM beam based on unified and integrated of Timoshenko's theory. *Compos. Struct.* **2020**, *242*, 112130. [CrossRef]

28. Sahu, N.K.; Biswal, D.K.; Joseph, S.V.; Mohanty, S.C. Vibration and damping analysis of doubly curved viscoelastic-FGM sandwich shell structures using FOSDT. *Structures* **2020**, *26*, 24–38. [CrossRef]

29. Andraș, A.; Radu, S.M.; Brînaș, I.; Popescu, F.D.; Budilică, D.I.; Korozsi, E.B. Prediction of Material Failure Time for a Bucket Wheel Excavator Boom Using Computer Simulation. *Materials* **2021**, *14*, 7897. [CrossRef] [PubMed]

30. Singh, A.; Nawayseh, N.; Dhabi, Y.K.; Samuel, S.; Singh, H. Transforming farming with intelligence: Smart vibration monitoring and alert system. *J. Eng. Res.* **2023**, *12*, 190–199. [CrossRef]

31. Yao, L.; Yuan, H.; Zhu, Y.; Jiang, X.; Cao, W.; Ni, J. Design and Testing of a Wheeled Crop-Growth-Monitoring Robot Chassis. *Agronomy* **2023**, *13*, 3043. [CrossRef]

32. Wang, X. *Finite Element Method*; Tsinghua University Press: Beijing, China, 2003.

33. Patrik, K.; Ramon, H.; Baerdemaeker, J.D. Modelling the Effect of Passive Vertical Suspensions on the Dynamic Behaviour of Sprayer Booms. *J. Agric. Eng. Res.* **1999**, *72*, 217–229. [CrossRef]

34. Qiu, B.; He, Y.; Sheng, Y.; Yin, Z.; Deng, W. Finite Element Modal Analysis and Structure Optimization of Spray Boom. *Trans. Chin. Soc. Agric. Mach.* **2014**, *45*, 112–116. [CrossRef]

35. He, Y.; Qiu, B.; Yang, Y.; Ma, J. Deformation analysis and control of elastic deformation for spray boom based on finite element model. *Trans. Chin. Soc. Agric. Eng.* **2014**, *30*, 28–36. [CrossRef]

36. Chen, D. *Study on Flexible Truss Boom System Design and Dynamic Simulation*; China Academy of Agricultural Mechanization Sciences: Beijing, China, 2011.

37. Chen, S.; Han, H.; Chen, G.; Shao, J.; Yao, Y. Dynamic characteristic analysis and vibration reduction design for sprayer frame. *Trans. Chin. Soc. Agric. Mach.* **2013**, *44*, 50–53. [CrossRef]

38. Yuan, H.; Yang, J.; Jiang, X.; Zhu, Y.; Cao, W.; Ni, J. Design and testing of a crop growth sensor aboard a fixed-wing unmanned aerial vehicle. *Comput. Electron. Agric.* **2022**, *194*, 106762. [CrossRef]

39. Ni, J.; Dong, J.; Zhang, J.; Pang, F.; Cao, W.; Zhu, Y. The spectral calibration method for a crop nitrogen sensor. *Sens. Rev.* **2016**, *36*, 48–56. [CrossRef]

40. Nolan, D.R.; Lally, C.; McGarry, J.P. Understanding the deformation gradient in Abaqus and key guidelines for anisotropic hyperelastic user material subroutines (UMATs). *J. Mech. Behav. Biomed. Mater.* **2022**, *126*, 104940. [CrossRef] [PubMed]

41. Abaqus Analysis User's Guide. 2019. Available online: https://130.149.89.49:2080/v6.14 (accessed on 15 March 2021).

42. Scotford, I.M.; Miller, P.C.H. Estimating Tiller Density and Leaf Area Index of Winter Wheat using Spectral Reflectance and Ultrasonic Sensing Techniques. *Biosyst. Eng.* **2004**, *89*, 395–408. [CrossRef]

43. Scotford, I.M.; Miller, P.C.H. Combination of Spectral Reflectance and Ultrasonic Sensing to monitor the Growth of Winter Wheat. *Biosyst. Eng.* **2004**, *87*, 27–38. [CrossRef]

44. Herrmann, I.; Vosberg, S.K.; Ravindran, P.; Singh, A.; Chang, H.-X.; Chilvers, M.I.; Conley, S.P.; Townsend, P.A. Leaf and Canopy Level Detection of Fusarium Virguliforme (Sudden Death Syndrome) in Soybean. *Remote Sens.* **2018**, *10*, 426. [CrossRef]

45. Xue, L.; Li, G.; Qin, X.; Yang, L.; Zhang, H. Topdressing nitrogen recommendation for early rice with an active sensor in south China. *Precis. Agric.* **2014**, *15*, 95–110. [CrossRef]

46. Yao, Y.; Miao, Y.; Cao, Q.; Wang, H.; Martin, L.G.; Georg, B.; Rajiv, K.; Yang, W.; Liu, F.; Liu, C. In-Season Estimation of Rice Nitrogen Status with an Active Crop Canopy Sensor. *IEEE J. Sel. Top. Appl. Earth Obs. Remote Sens.* **2014**, *7*, 4403–4413. [CrossRef]

47. Ali, A.M.; Thind, H.S.; Singh, V.; Singh, B. A framework for refining nitrogen management in dry direct-seeded rice using GreenSeeker™ optical sensor. *Comput. Electron. Agric.* **2015**, *110*, 114–120. [CrossRef]

48. Yu, K.; Li, F.; Martin, L.G.; Miao, Y.; Georg, B.; Chen, X. Remotely detecting canopy nitrogen concentration and uptake of paddy rice in the Northeast China Plain. *ISPRS J. Photogramm. Remote Sens.* **2013**, *78*, 102–115. [CrossRef]

49. Cordero, E.; Moretti, B.; Francesca, M.E.; Tenni, D.; Beltarre, G.; Romani, M.; Sacco, D. Fertilisation strategy and ground sensor measurements to optimise rice yield. *Eur. J. Agron.* **2018**, *99*, 177–185. [CrossRef]